Influence of nanometric CeO_2 coating on high temperature oxidation of Cr*

Jin Huiming[1**], Zhang Linnan[2] and Liu Xiaojun[2]

(1. Materials Research Center, Department of Mechanical Engineering, Yangzhou University, Yangzhou 225009, China; 2. College of Materials Science and Engineering, North-East University, Shenyang 110014, China)

Accepted on October 18, 2006

Abstract Isothermal and cyclic oxidation behavior of chromium and its superficially applied nanometric CeO_2 samples were studied at 900℃ in air. Scanning electronic microscopy (SEM), transmission electronic microscopy (TEM) and high resolution electronic microscopy (HREM) were used to examine the morphology and micro-structure of oxide films. It was found that ceria addition greatly improved the anti-oxidation ability of Cr both in isothermal and cyclic oxidizing experiments. Acoustic emission (AE) technique was used *in situ* to monitor the cracking and spalling of oxide films, and AE signals were analyzed in time-domain and number-domain according to the related oxide fracture model. Laser Raman spectrometer was also used to study the stress status of oxide films formed on Cr with and without ceria. The main reason for the improvement in anti-oxidation of chromium was that ceria greatly reduced the growing speed and grain size of Cr_2O_3. This fine-grained Cr_2O_3 oxide film might have better high temperature plasticity and could relieve parts of compressive stress by means of creeping, and maintained the ridge character and relatively low internal stress level. Meanwhile, ceria application reduced the size and the number of interfacial defects, while remarkably enhanced the adhesive property of Cr_2O_3 oxide scale formed on Cr substrate.

Keywords: oxidation, stress, CeO_2 nanoparticle coating, chromium.

The resistance of metals to high temperature oxidizing environment depends on the formation and maintenance of a slowly growing and adherent oxide scale. Usually there were internal growing stress and external thermal stress in the oxide film. The former might arise from the volume changes when the metal was oxidized to oxide, while the latter might arise from the thermal expansion difference between the metal and the oxides. When the stress in the oxide scale reaches a critical value, the oxide film might buckle or spall as results of the propagation of microcracks. These stress-related phenomena occurred especially at the metal-oxide interface[1,2]. Usually, the addition of a small amount of rare earth elements in metals substrate can improve the anti-oxidation property of metals, while the rare earth effect (REE) has not been fully understood yet[3—9]. In this paper, the oxidation kinetics of chromium and its superficially applied nano-CeO_2 samples, the residual stress and the adhesive property of oxide films are studied by several methods.

1 Experiment

Pure (99.94% mass content) chromium was wire-cut to 15 mm × 10 mm × 2 mm specimens which were finally polished by 0.2 μm Al_2O_3 abrasive paste. Nano-CeO_2 (20 nanometer in average diameter) in alcohol solution (30 g/L) was prepared in ultra-sonic bath, and some specimens were dipped in this solution and then dried in air. Specimens with and without ceria were isothermally oxidized for 50 hours at 900℃ in air to examine the oxidizing kinetics in SETTRAM-50 thermal gravity analyzing (TGA) equipment. These specimens were also cyclically oxidized (50 min heating and 10 min air-cooling per cycle) for 90 hours to examine the respective mass changes. Scanning electronic microscopy (SEM), transmission electronic microscopy (TEM) and high resolution electronic microscopy (HREM) were used to examine oxide films.

In acoustic emission (AE) test, specimens were point-welded to one end of a Pt wave-guide (1 mm in diameter) and oxidized in furnace, and the other end of the wave-guide was attached to a pre-amplifier which was connected with AE-100 acoustic emission system. Each specimen was isothermally oxidized for 20 hours in furnace and then naturally cooled. During the whole procedure AE signals were recorded. The

* Supported by National Natural Science Foundation of China (Grant No. 29231011) and Natural Science Foundation of Jiangsu Province (Grant No. 04KJD460010)

** To whom correspondence should be addressed. E-mail: doctorjhm@sohu.com

total signal-gain was set to be 86 dB in the AE system, and the threshold voltage was set to be 1.2 V.

In Raman test Hitachi RM-200 Spectrum was used to examine the Raman peak shift of surface oxides. Ar^+-Laser tube was used and the Raman peak was calibrated to an accuracy of ± 0.2 cm^{-1}.

2 Results

The isothermal oxidation mass gain curves of chromium and its nano-CeO_2 applied samples are shown in Fig. 1. It can be seen that CeO_2 application reduced the isothermal oxidizing rate of chromium.

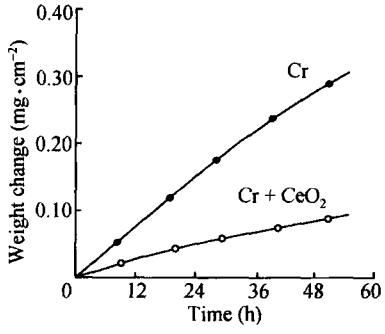

Fig. 1. Isothermal oxidation mass gain curves of pure Cr and CeO_2 applied Cr.

Fig. 2(a) shows the surface morphology of CeO_2 coated sample before oxidation. Fig. 2(b) and Fig. 2 (c) shows oxides formed on CeO_2-free and CeO_2-coated samples after 50 hours of isothermal oxidation. We can see that CeO_2 application remarkably reduced the Cr_2O_3 grain size and introduced apparent ridge character in oxide film.

The cyclic oxidation mass gain curves of Cr and its CeO_2 applied samples are shown in Fig. 3. It can be seen that Cr_2O_3 film formed on pure Cr began to spall after 22 hours of cyclic oxidation and showed weight loss, while the CeO_2 applied sample showed no spallation or weight loss during the whole experiment stage.

Acoustic emission testing results of both samples are shown in Fig. 4. At the isothermal oxidizing stage, no AE signal was detected, while at the subsequent naturally cooling stage lots of AE signal were detected (Fig. 4(a) and (b)), which means cracking and/or spalling (stress-release related) happened in the oxide film or at the oxide/metal interface[7,8]. The initial temperatures at which AE signal began to arise for pure Cr and CeO_2 applied Cr were 880℃ and 320℃ respectively.

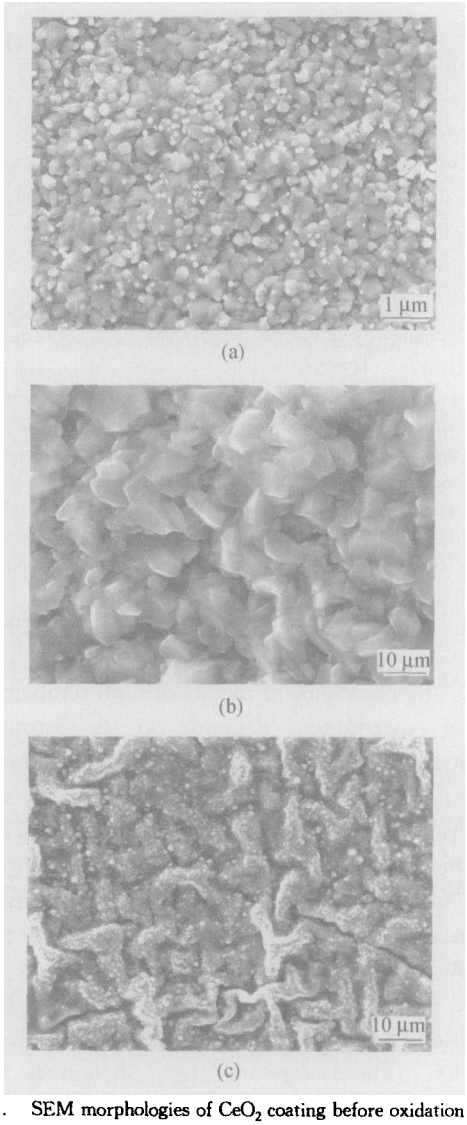

Fig. 2. SEM morphologies of CeO_2 coating before oxidation (a), oxide scales formed on pure Cr (b) and CeO_2 coated Cr (c) after oxidation.

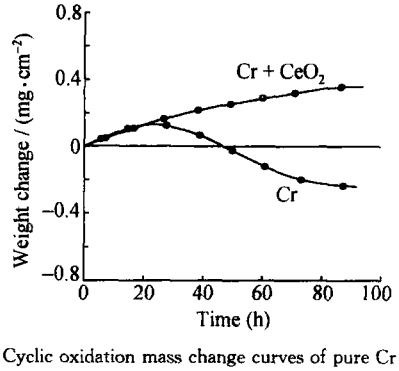

Fig. 3. Cyclic oxidation mass change curves of pure Cr and CeO_2 coated Cr.

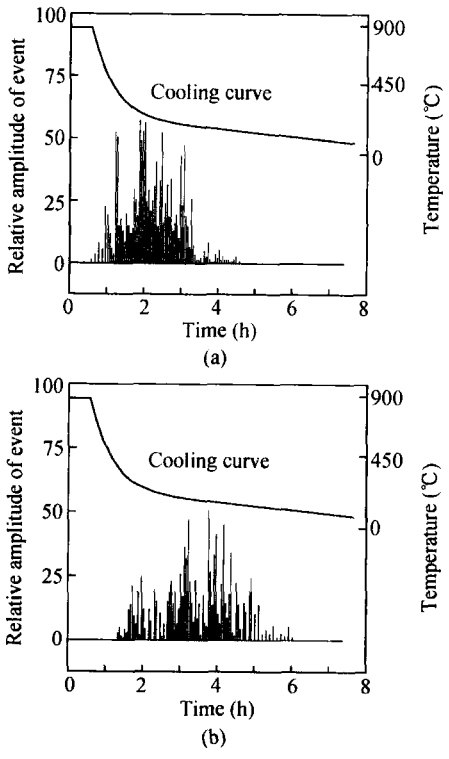

Fig. 4. AE events distribution on pure Cr (a) and CeO_2 coated Cr (b).

In the Raman experiment, pure fine grain-sized Cr_2O_3 powder was annealed at 850℃ for 40 hours and was considered as the standard stress-free status of Cr_2O_3 oxide (Fig. 5(a))[10]. The Raman peaks of Cr_2O_3 oxides formed on Cr and CeO_2 applied Cr are shown in Fig. 5(b) and (c) respectively.

According to Birnie's work[12], mono-chromatic Laser light was inelastically scattered to give Raman spectrum corresponding to particular molecular and lattice vibrations of solid. When a sample was stressed, the vibration frequencies of the Raman peaks shifted to higher frequency for a compressive stress. From Fig. 5 we could see that CeO_2 application reduced the compressive stress level in Cr_2O_3 oxide film.

3 Discussion

According to Ref. [1], the oxide film spalling process should be preceded by the film buckling process above an interfacial defect. When the accumulative compressive stress inside the oxide film reaches a critical value, oxide film buckling will occur above interfacial defects. The compressive stress in the buckled region is partially relieved, and the concentrated stress at the perimeter of this buckled region will cause propagation of crack tip towards the outer face of oxide film, and finally result in through-thickness cracking and spalling of oxide film. This process is schematically shown in Fig. 6.

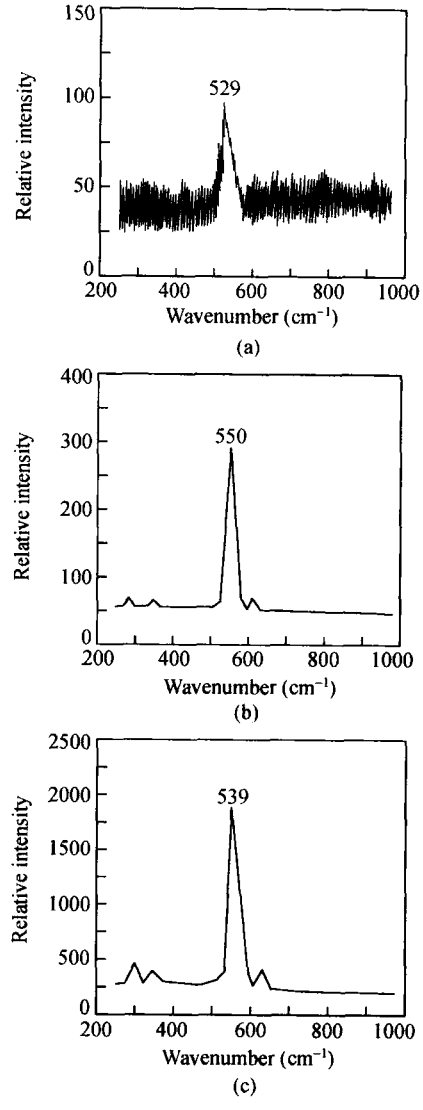

Fig. 5. Raman peaks of standard Cr_2O_3 powder (a), oxides formed on pure Cr (b) and CeO_2 coated Cr (c).

During the isothermal oxidizing stage, the growth stress σ_{gw} caused by volume change can be correlated to *Pilling-Bedworth ratio* (PBR) (volume of oxide/volume of metal consumed). During the air-cooling stage, the thermal stress σ_{th} was generated due to the linear thermal expansion difference between oxide and substrate metal. According to Evans and Zhang's film fracture model[2,6], the quantitative description for the critical stress condition could be expressed as

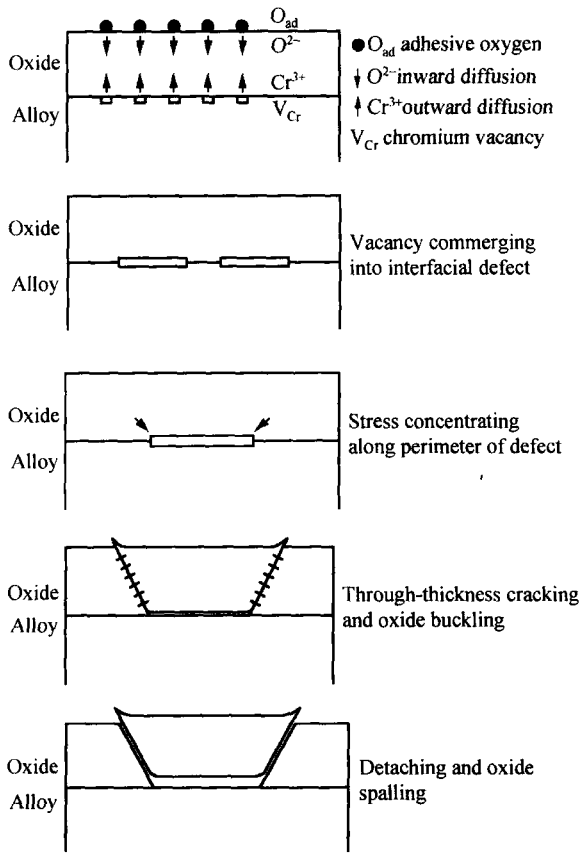

Fig. 6. Schematic diagram of interfacial defect formation and cracking and spalling of oxide film upon interfacial defect.

$$\sigma_{OX} = \frac{3.6H^2E_{OX}}{C^2} \quad (1)$$

$$C = 1.9H\left(\frac{(1-\nu)}{\Delta T(\alpha_M - \alpha_{OX})}\right)^{1/2} \quad (2)$$

$$N = \frac{1}{Z}f\left(3.6\frac{H^2(1-\upsilon)\Delta T}{C^2(\alpha_M - \alpha_{OX})}\right) \quad (3)$$

Here, H is the thickness of oxide film, σ_{OX} is the internal stress in oxide, E_{OX} is the *Young*'s modulus of oxide, ν is the *Poisson*'s ratio of the oxide, α_M and α_{OX} are the thermal expansion coefficient of the metal and oxide respectively, C and N are the size and the number of oxide/metal interfacial defect respectively, ΔT is temperature change, Z is an integer between 5 and 8 according to Zhang's work[5], f is the differential function of AE event number in the temperature domain.

By converting the measured distribution of AE signals (Fig. 4) in time domain to temperature domain using Hi-Draw2.1 software in AE-100 acoustic emission apparatus and by differential calculation of the number of AE signals on temperature domain using equation (1), (2) and (3), we can finally get the interfacial defect number distribution (N) *vs* defect size (i.e. radius C) as shown in Fig. 7. Detailed description of the above three equations and mathematical method were reported in Refs. [5] and [9].

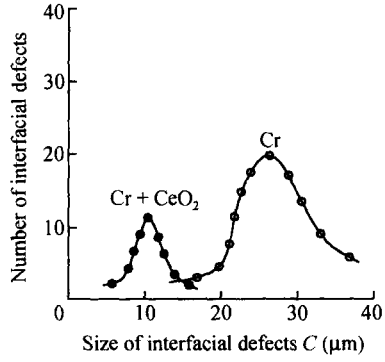

Fig. 7. Number distribution of interfacial defects of pure Cr and CeO_2 coated Cr.

From Fig. 7 we can find that the interfacial defects' number distribution *vs* defect size is roughly by law of Gauss' distribution, and the average interfacial defect radius for Cr and CeO_2 applied Cr are 27.5 μm and 11.0 μm respectively. Meanwhile nano-CeO_2 application has reduced the total number of interfacial defects, which can be seen by comparing the areas under the two distributional curves in Fig. 7.

Nano-CeO_2 application greatly reduced the isothermal oxidizing rate of Cr as shown in Fig. 1 and refined the Cr_2O_3 oxide size. This kind of fine-grained oxide film could have better high temperature plasticity and creeping property, which meant oxide film could relieve parts of internal stress by means of high temperature creeping rather than by means of cracking and spalling[11,13]. The characteristic ridges formed on CeO_2 applied Cr_2O_3 oxide film (Fig. 2(b)) were the results and proof of high temperature creeping of the fine-grained oxide film.

Fig. 8 is the TEM bright field image and HREM images of Cr_2O_3 film formed on nano-CeO_2 applied samples. We could find that CeO_2 application greatly refined the oxide film to micro-crystal structure (see the typical diffraction rings in Fig. 8(a)), and nano-CeO_2 particles had sintered with Cr_2O_3 grain during the oxidizing process (Fig. 8(b)).

Additionally, CeO_2 application remarkably reduced the number and size of interfacial defects as shown in Fig. 7 and improved the Cr_2O_3/Cr interfa-

cial adhesive property. The acoustic emission technique used in our experiment to examine the spalling and cracking of oxide film seemed to be a promising method in quantitatively studying the oxide/metal interfacial behavior, although it had some drawbacks and deviation[5,9].

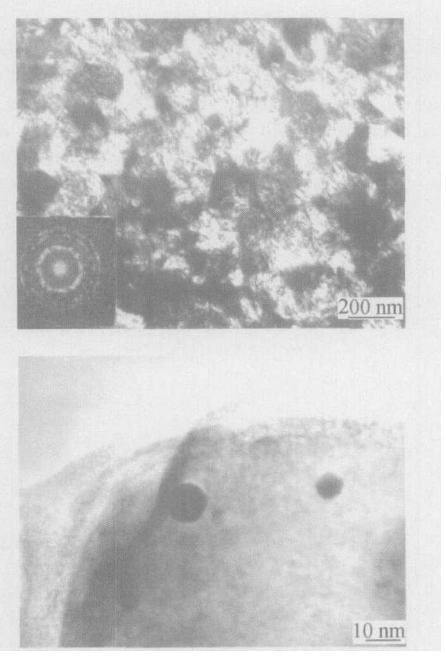

Fig. 8. TEM bright field image(a) and HREM images of CeO_2 coated Cr_2O_3 oxide film (b).

The overall effects of nano-CeO_2 application on oxidation of Cr were similar to that of yttrium ion-implantation on oxidation of Cr and Co—40Cr binary alloy, such as the ridge character, the reduction in oxidizing rate, the micro-crystal structure and the improved adhesive property. In the ion-implantation case, the rare earth element with high local concentration and high chemical activity was doped in metal's surface, and caused large amounts of lattice defects[3]. This caused the oxide grain refining effect at the initial oxidizing stage (perhaps several seconds) and other effects (relating to ion-diffusion within film, tress lever, creeping property and adhesive property) at the later oxidizing stage[12,13].

CeO_2 apparently had no such effect at the initial oxidizing stage, the only possible reason for all the effects found in our experiment was that nano-CeO_2 sintered with Cr_2O_3 oxide and inter-diffusion existed between these two oxides due to their semi-conductor nature. Consequently the oxidizing mechanism might change from predominant cation outward diffusion to predominant anion inward diffusion[2,3] as occurring in the ion-implanting case. Few work had been reported on the sintering mechanism except Przybilla[7] and Ul-Hamid[10], who used field emission electronic microscopy with energy dispersive spectrum (FEEM/EDS) to examine the actual existing form of rare earth element within oxide films. Besides the very fine Y_2O_3, CeO_2 and $YCrO_3$ spinel phases, they found that rare earth elements might also segregate to Cr_2O_3 oxide grain boundaries in the forms of Y^{3+} and Ce^{4+} ions. The electron beam' diameter was 1 nm in their equipment and common TEM, and HREM were unable to fulfill element detection with EDS at such high apace resolution and accuracy. In our previous work[4,9], we studied the segregating process and existing form of yttrium in Cr_2O_3 oxide in the ion-implantation case. Further studies are still needed to explain the sintering process and interaction mechanism of nano-CeO_2 with Cr_2O_3 oxide as well as the overall rare earth effects (REE) in our experiment.

4 Conclusions

(i) Nano-CeO_2 application remarkably lowered the isothermal oxidizing rate of chromium at 900℃ in air. Meanwhile, Cr_2O_3 oxide' grain-size was much reduced and had ridge characterization due to CeO_2 application.

(ii) Adhesion of Cr_2O_3 film was greatly improved via CeO_2 application. This was due to the film's better high temperature plasticity, creeping ability and relatively small internal stress.

(iii) Acoustic emission tests showed that the number and average size of interfacial defects reduced due to CeO_2 application. The overall rare earth effects of nano-CeO_2 superficial application were caused not at the initial oxidizing stage as in the case of ion-implantation, but at the later oxidizing stage during which nano-CeO_2 sintered with Cr_2O_3. Actual sintering process and interactive mechanism between two oxides need further studies.

References

1 Evans AG and Cannon R. Stress and decohesion of oxide scales. Materials Science Forum, 1989, 43(3): 243—249
2 Evans HE. Cracking and spalling of protective oxide layers. Materials Science and Engineering, 1989, A120(10): 139—146
3 Rahmel A and Schutze M. Mechanical aspects of rare earth effects. Oxidation of Metals, 1992, 38(2): 314—319

4 Jin HM, Zhang LN, Li MS, et al. Rare earth effects on adhesion of Cr_2O_3 oxide scale formed on surface of Co—40Cr alloy. Journal of Rare Earths, 2001, 19(1): 34—38

5 Zhang YF, Shores D, Rahmel A, et al. Spallation of oxide scales formed on Ni—30Cr alloy. Oxidation of Metals, 1993, 40(1): 529—536

6 Vasyliv BD. Initiation of a crack from the edge of a notch with oblique front in specimens of brittle materials. Journal of Materials Science, 2002, 38(5): 724—728

7 Przybilla W and Schutze M. Role of growth stresses on the structure of oxide scales on nickel at 800 and 900℃. Oxidation of Metals, 2002, 58(1): 103—145

8 Hou PU and Stringer J. The influence of ion implanted yttrium on the selective oxidation of chromium in Co—25Cr. Oxidation of Metals, 1988, 29(8): 45—51

9 Jin HM, Felix AC and Aroyave MH. Rare earth effect yttrium on formation and property of Cr_2O_3 oxide film formed on Co—Cr binary alloy. Progress in Natural Science, 2006, 16(1): 72—77

10 Ul-Hamid A. Study of the effect of Y on the scale microstructures of Cr_2O_3— and Al_2O_3—forming alloys. Oxidation of Metals, 2002, 58(1): 23—45

11 Birnie J and Cragga C. *Ex situ* and *in situ* determination of stress distribution in chromium oxide films by Raman microscopy. Corrosion Science, 1992, 33(2): 1—12

12 Seal S, Kuiry SC and Bracho LA. Studies on the surface chemistry of oxide films formed on IN738 superalloy at elevated temperature. Oxidation of Metals, 2001, 56(5): 583—603

13 Kloss B and Wenderoth M. Fast internal oxidation of Ni—Zr—Y alloys at low oxygen pressure. Oxidation of Metals, 2004, 61(3): 239—251